

Effect of solvents on electrochemical performance of polypyrrole coated LiFePO₄/C cathode materials for Li-ion battery

Rajeev Sehrawat¹ · Anjan Sil¹

Received: 5 February 2015 / Accepted: 4 April 2015 / Published online: 14 April 2015
© Springer Science+Business Media New York 2015

Abstract The effect of the nature of solvent on polypyrrole (PPy) synthesis by in situ coating on the prior synthesized carbon coated LiFePO₄ for electrochemical properties of composite materials designated as LiFePO₄/C-PPy has been investigated. An in situ chemical oxidation method is used for the polymerization of pyrrole by using three different solvents e.g. water, ethanol and acetonitrile (ACN). The structure and morphology of PPy grown as coating is characterized by Raman spectroscopy and scanning electron microscopy respectively. X-ray diffraction patterns of the composites confirm the presence of Li_{0.05}FePO₄ compound as a minor phase along with major LiFePO₄ phase. The ACN assisted synthesized PPy coating shows best electrochemical performance as cathode material among selected solvents used for the synthesis. Electrochemical impedance spectroscopy indicates lowest electrode impedance and highest Li-ion diffusion for the composite LiFePO₄/C-PPy synthesized in ACN solvent as compared to the water and ethanol derived samples. The higher rate capability (82 mAh g⁻¹) of the composite LiFePO₄/C-PPy synthesized in ACN solvent as compared to LiFePO₄/C (42 mAh g⁻¹), is attributed to the morphology and structure of the polymer coating.

1 Introduction

The use of LiFePO₄ as cathode material for rechargeable lithium ion batteries has been increasing in many applications like small scale electronic devices to electric vehicle (EV) or hybrid electric vehicle. The LiFePO₄ cathode material has several advantages such as they are non-toxic, inexpensive, environment friendly and have flat discharge voltage at 3.4 V versus Li/Li⁺ and good theoretical charge capacity of 170 mAh g⁻¹ [1, 2]. But the material LiFePO₄ does not provide good rate capability as it has poor electronic conductivity ($\sim 10^{-9}$ S cm⁻¹) and low ionic diffusivity (10^{-17} – 10^{-14} cm² s⁻¹) [3]. Many efforts have been made by the researchers to improve the electronic conductivity and ionic diffusivity of the LiFePO₄ material. Surface coating and doping of the oxide particles are proved to be effective to achieve good conductivity of the material [4, 5]. Carbon coating has been used to improve the conductivity of LiFePO₄, but one of the major drawbacks is that the carbon is electrochemically inactive and therefore leads to decrease the volumetric energy density of the electrode [6]. Conducting polymer coating around LiFePO₄ particles have improved rate capability of LiFePO₄ [7].

PPy shows the electronic conductivity due to delocalization of pie-electrons in the conjugated pie-bond system [8]. The conductivity of the synthesized PPy can further be improved by using suitable solvent and doping with organic dopant sodium p-toluene sulfonate (Na-PTSA) or inorganic dopants ClO₄⁻, BF₄⁻ and NO₃⁻ [8, 9]. The doping with Na-PTSA as compared to inorganic dopants results in good and stable electronic conductivity of PPy [10].

In the present study, PPy is synthesized using different solvents viz. water, ethanol and ACN. The study has indicated that ACN solvent derived PPy coating on LiFePO₄/C has highest specific capacity. The polarity of

✉ Rajeev Sehrawat
rajeev.sehrawat@gmail.com

¹ Department of Metallurgical and Materials Engineering,
Indian Institute of Technology Roorkee, Roorkee 247667,
India

solvent used for the polymerization affects the morphology of PPy [11].

2 Experimental

2.1 Synthesis of carbon coated LiFePO₄

The synthesis of carbon coated LiFePO₄ (designated as LiFePO₄/C) was carried out in two steps. In the first step, 1.0 ml of aniline monomer (99.5 %, GR, Merck) and 2.62 g of (NH₄)₂(PO₄) (99 %, GR, Merck) are mixed in 200 ml of Millipore water. A dropwise addition of 100 ml of aqueous solution of 3.7 g of FeCl₃ (98 %, Merck) was made into the previous mixture. White colored FePO₄ precipitate forms instantaneously in the solution. The solution which initially was white in color slowly becomes light green because of the formation of polyaniline on the surface of FePO₄ particles 4 h after the addition of aqueous solution of FeCl₃. In the second step, the synthesized material in the powder form was ground in a pestle-mortar with Li(CH₃COO) (99 %, Loba chemie.) powder maintaining molar ratio of 1:1 between Li and Fe. The mixture was heated at 400 °C for 4 h under the Ar-10 % H₂ gas atmosphere before calcination and was further grinded in a pestle-mortar for 30 min to homogenize the mixture. The material was again heated at 700 °C for 15 h under Ar-10 % H₂ atmosphere for calcination. The calcined material was further washed thoroughly in deionized water and acetone to remove chlorine to get pure LiFePO₄/C powder.

2.2 Synthesis of PPy

For synthesizing PPy, three suspensions each were containing 1 ml of pyrrole monomer in 40 ml of each solvent (water, ethanol and ACN) were made separately and stirred at 0–5 °C. In each suspension 0.95 g of Na-PTSA was added. Further 7.25 g of FeCl₃ dissolved in 20 ml of corresponding solvent was added dropwise in the above suspensions prepared. The color of the solution changes from transparent to black on the addition of FeCl₃ solution showing the formation of PPy precipitates inside the suspension. The molar ratio of the additive Na-PTSA to pyrrole was 1:3 and oxidizing agent to pyrrole was kept at 3:1 [12]. The reaction was carried out for 4 h with continuous stirring. After 4 h the solution was filtered and washed with their respective solvents used. The filtered material was dried in vacuum oven for 12 h at 60 °C.

2.3 Synthesis of LiFePO₄/C-PPy composite

For the synthesis of LiFePO₄/C-PPy composites, 1 g of LiFePO₄/C powder added in 40 ml solvent each of water,

ethanol and ACN were sonicated for 15 min to prepare the suspensions. 1 ml of pyrrole monomer was added in each suspension under continuous stirring between 0 and 5 °C. After homogenization for 15 min with continuous stirring, 0.95 g of Na-PTSA was added in the above suspensions followed by the addition of FeCl₃ (7.25 g) dissolved in corresponding solvents to each suspension. After 4 h of polymerization the solutions were filtered and washed with the corresponding solvents. The synthesized materials were dried in vacuum oven for 12 h at 60 °C to get the LiFePO₄/C-PPy composite. The LiFePO₄/C-PPy composite materials synthesized in each of ACN, ethanol and water solvents were designated as LiFePO₄/C-PPy(ACN), LiFePO₄/C-PPy(ethanol) and LiFePO₄/C-PPy(water).

2.4 Physical characterizations

XRD patterns of the LiFePO₄ and LiFePO₄/C-PPy composites were obtained using a Bruker (AXS, D8 advance) X-ray diffractometer using X-ray radiation ($\lambda_{\text{CuK}\alpha} = 1.5406 \text{ \AA}$) with a scanning rate of 1.5 °/min. The morphologies of samples were observed by field emission transmission electron microscope (TEM, FEI-TECHNAI-20) and field emission scanning electron microscope (SEM, FEI Quanta 200F). The PPy contents in the samples were estimated by thermogravimetric analysis of the samples using thermal analyzer (Seiko Instruments, EXSTAR TG/DTA 6300). Raman confocal micro-spectrometer system (inVia, Renishaw) was used to characterize the carbon coating on the samples for its graphitization and confirming the formation of PPy in the LiFePO₄/C-PPy composites. He–Ne LASER beam having wavelength of 514 nm as the excitation source was used to obtain Raman spectra of the synthesized materials.

2.5 Electrochemical characterization

The slurries were prepared with active material, acetylene black, and PVDF binder in the proportion (in weight %) of 70:15:15 respectively mixed in the NMP solvent. For preparation of the electrode aluminum foil was coated with the slurry. The coating was dried under vacuum at 120 °C for 24 h. The dried coating was pressed using a hydraulic press at a pressure of 500 kN m⁻² to ensure good adherence of the paste material with the aluminium foil. The coated foils were cut into the required size of the working electrode. The counter electrode of lithium metal and working electrode were assembled in a laboratory fabricated Teflon cell inside the glove box under high purity argon atmosphere having controlled moisture and oxygen contents of <0.1 ppm. The complete Teflon cell assembly consists of a cathode (working electrode), an anode (lithium metal foil), a polypropylene microporous separator

membrane soaked with a liquid electrolyte of 1 mol L⁻¹ LiPF₆ dissolved in a 1:1 v/v solution of dimethyl carbonate (DMC) and ethylene carbonate (EC). The electrochemical and cyclic voltammetry tests were performed using a battery testing system (BT2000, Arbin Instruments). The cell was charged and discharged galvanostatically over the voltage range between 2.2 and 4.2 V (vs. Li/Li⁺) at different current rates. Electrochemical impedance spectroscopy (EIS) analyses of the cells were carried out on the electrochemical workstation (Gamry Instruments) in the frequency range from 0.1 Hz to 100 kHz and at a voltage of 0.5 mV.

3 Results and discussions

3.1 XRD-analysis

Figure 1 shows the XRD-patterns of LiFePO₄/C and LiFePO₄/C-PPy composite materials. All the diffraction peaks for the sample LiFePO₄/C can be indexed according to the diffraction pattern of LiFePO₄ having olivine-orthorhombic structure (JCPDS card No. 01-083-2092) and space group Pnma (62). The diffraction pattern of the composite LiFePO₄/C-PPy shows that material consists of two phases of LiFePO₄ (JCPDS file No. 01-083-2092) and Li_{0.05}FePO₄ (JCPDS file No. 98-10-8284). The formation of Li_{0.05}FePO₄ phase implies that lithium depletion has taken place due to the lithium extraction by the polymer coating of PPy because the polymer is electrochemically active. Both the phases of LiFePO₄ and Li_{0.05}FePO₄ are reported to have same capacity [13]. The characteristic peaks of carbon and PPy are not visible in the XRD patterns (Fig. 1) which imply that the PPy coating is

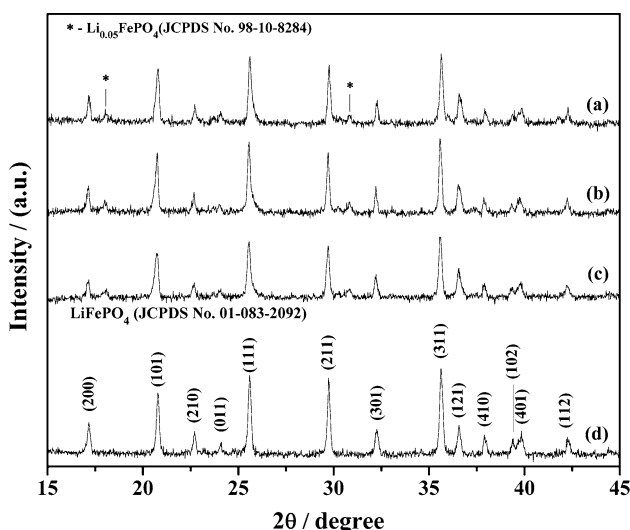


Fig. 1 XRD patterns of *a* LiFePO₄/C-PPy(ACN), *b* LiFePO₄/C-PPy(ethanol), *c* LiFePO₄/C-PPy(water) and *d* LiFePO₄/C

amorphous and carbon content in the materials is sufficiently low. Moreover, a fraction of the carbon is of disordered form that is confirmed by Raman spectroscopic analysis of the sample.

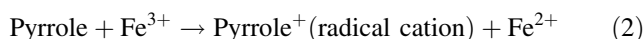
The Table 1 shows the major peak positions and intensities of Li_{0.05}FePO₄ (JCPDS file No. 98-10-8284) and LiFePO₄ (JCPDS file No. 01-083-2092). The resolved and unresolved peaks of Li_{0.05}FePO₄ in the observed XRD pattern are also indicated.

3.2 Thermal analysis

Figure 2 shows the TG profiles of the samples LiFePO₄/C-PPy(water), LiFePO₄/C-PPy(ethanol), LiFePO₄/C-PPy(ACN) and pristine PPy heated at the rate of 10 °C min⁻¹ from room temperature to 800 °C at which the materials were held for 1 h to remove the PPy content completely by decomposition. A nominal weight loss was occurred over the temperature range up to 120 °C in all the samples because of the removal of water molecules from the samples. Above 120 °C, a gradual weight loss of the materials take place up to 800 °C due to decomposition of PPy coating. The steep fall in the weight at 800 °C is due to decomposition of PPy at that temperature. The polymer content in LiFePO₄/C-PPy(water), LiFePO₄/C-PPy(ethanol), LiFePO₄/C-PPy(ACN) were estimated as 6.9, 5.5 and 6.6 wt% respectively.

3.3 Morphology of LiFePO₄/C-PPy

SEM micrographs of the pristine PPy, LiFePO₄/C and LiFePO₄/C-PPy composites are shown in Fig. 3. The Fig. 3a, b show the morphologies of pristine PPy synthesized in ACN and water respectively. The PPy powder prepared in ACN solvent has low porosity and smooth surface than that of powder synthesized in water. The polymerization process involves the formation of radical cation of pyrrole due to its oxidation by FeCl₃.



During polymerization the Pyrrole radical cation combines with other similar radical cation for chain propagation of the polymer. But if the polymer synthesis is processed in water or ethanol the active centers of the growing chain were attacked by the -OH and C = O nucleophilic groups instead of other free pyrrole radical [14]. Due to the attack of -OH and C = O, PPy chains become hydrophobic to the solvent resulting in the lowering of active centers and formation of aggregates of PPy. So, the PPy synthesized in the water or ethanol solvents have more porosity and surface roughness as compared to the ACN derived PPy [15].

Table 1 Peaks position and their respective relative intensities of $\text{Li}_{0.05}\text{FePO}_4$ (JCPDS file No. 98-10-8284) and LiFePO_4 (JCPDS file No. 01-083-2092)

S. no.	2θ ($^\circ$) for LiFePO_4	Peak intensity for LiFePO_4 ($I = I_{2\theta} \times 100/I_{\text{max}}$)	2θ ($^\circ$) for $\text{Li}_{0.05}\text{FePO}_4$	Peak intensity for $\text{Li}_{0.05}\text{FePO}_4$ ($I = I_{2\theta} \times 100/I_{\text{max}}$)	Peak status of $\text{Li}_{0.05}\text{FePO}_4$ in $\text{LiFePO}_4/\text{C-PPy}$ XRD pattern
1	17.17	38.0	18.04	69.4	Resolved
2	20.81	76.2	20.644	94.0	Unresolved
3	25.6	83.3	25.777	88.9	Unresolved
4	29.73	78.2	30.819	79.2	Resolved
5	35.61	100	36.663	100.0	Unresolved

The resolved and unresolved peaks of $\text{Li}_{0.05}\text{FePO}_4$

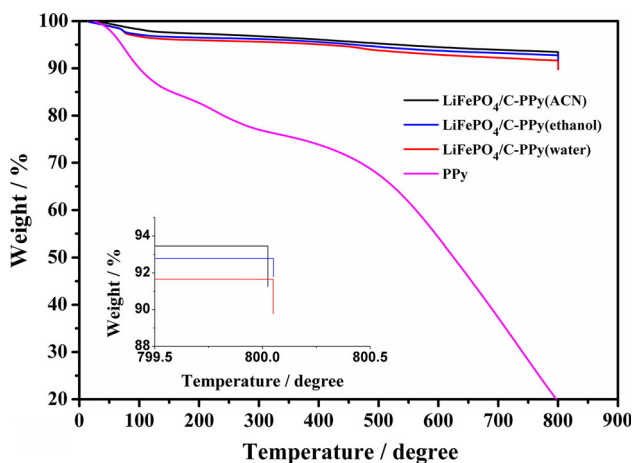


Fig. 2 TG plots of $\text{LiFePO}_4/\text{C-PPy}(\text{water})$, $\text{LiFePO}_4/\text{C-PPy}(\text{ethanol})$, $\text{LiFePO}_4/\text{C-PPy}(\text{ACN})$ and PPy measured at a heating rate of $10^\circ\text{C}/\text{min}$ in Argon gas atmosphere

The FESEM micrograph of LiFePO_4/C particles (Fig. 3f) shows that particles are nearly spherical having size range of 100–500 nm. The LiFePO_4/C particles are agglomerated through the carbon present on the surface of LiFePO_4 particles. Figure 3c–e show the SEM micrographs of the composites $\text{LiFePO}_4/\text{C-PPy}(\text{ACN})$, $\text{LiFePO}_4/\text{C-PPy}(\text{water})$ and $\text{LiFePO}_4/\text{C-PPy}(\text{ethanol})$ respectively. The micrographs show that the morphology of the PPy is same as that of pristine PPy synthesized in the corresponding solvents. The PPy in the composites $\text{LiFePO}_4/\text{C-PPy}(\text{water})$ and $\text{LiFePO}_4/\text{C-PPy}(\text{ethanol})$ partially make the coverage of the underneath materials component. It is also observed that the PPy chains grow separately in the coating region. The surface roughness and porosity of the PPy coating is higher in the $\text{LiFePO}_4/\text{C-PPy}(\text{water})$ and $\text{LiFePO}_4/\text{C-PPy}(\text{ethanol})$ as compared to that of $\text{LiFePO}_4/\text{C-PPy}(\text{ACN})$. The micrograph in Fig. 3c suggests that $\text{LiFePO}_4/\text{C-PPy}(\text{ACN})$ composite is largely covered by the PPy.

3.4 TEM analysis

Figure 4a, c show the TEM micrographs of LiFePO_4/C and $\text{LiFePO}_4/\text{C-PPy}(\text{ACN})$ composite powder materials. Figure 4b presents a high resolution micrograph of Fig. 4a to show the lattice fringes of the particle and gives the carbon coating thickness which was estimated to be 3 nm. The surface coverage of the LiFePO_4/C particles with the PPy is observed in the micrograph of Fig. 4c. Though the particles are seen present in the agglomerate state, however, the regular (nearly spherical) shape of the particles remains unchanged after surface coating with the polymer. An average size of all the $\text{LiFePO}_4/\text{C-PPy}$ composites particle is ~ 300 nm.

3.5 Raman spectra analysis

The structure of carbon and PPy coatings that developed on the LiFePO_4 particles is very important for assessing the electronic conductivity and Li-ion diffusivity of the LiFePO_4/C material. Raman analysis was performed to know the structure of carbon and PPy. The broad and high intensity bands at 1350 and 1580 cm^{-1} in Raman spectra of LiFePO_4/C signify the D and G-bands of carbon (Fig. 5). The D-band originates because of defects associated with finite graphene size such as edges with special shapes and atomic defect within a graphene layer, leading to break of symmetry in the structure [16]. The A_{1g} mode of vibration, occurs at the k_1 (edge) point of first Brillion zone that give rise to D-band. For the infinite graphitic size the change in polarizability is cancelled, therefore A_{1g} mode of vibration is Raman inactive. But for finite graphitic size polarizability change exists due to which graphitic carbon become, Raman active. So, the intensity at 1350 cm^{-1} was attributed to A_{1g} mode for finite size of graphitic carbon or at the edges of lager graphitic carbon [17]. While the G-band represents highly ordered graphitic carbon. Li et al. [18] have reported that the small intensity ratio ($R = I_D/I_G$)

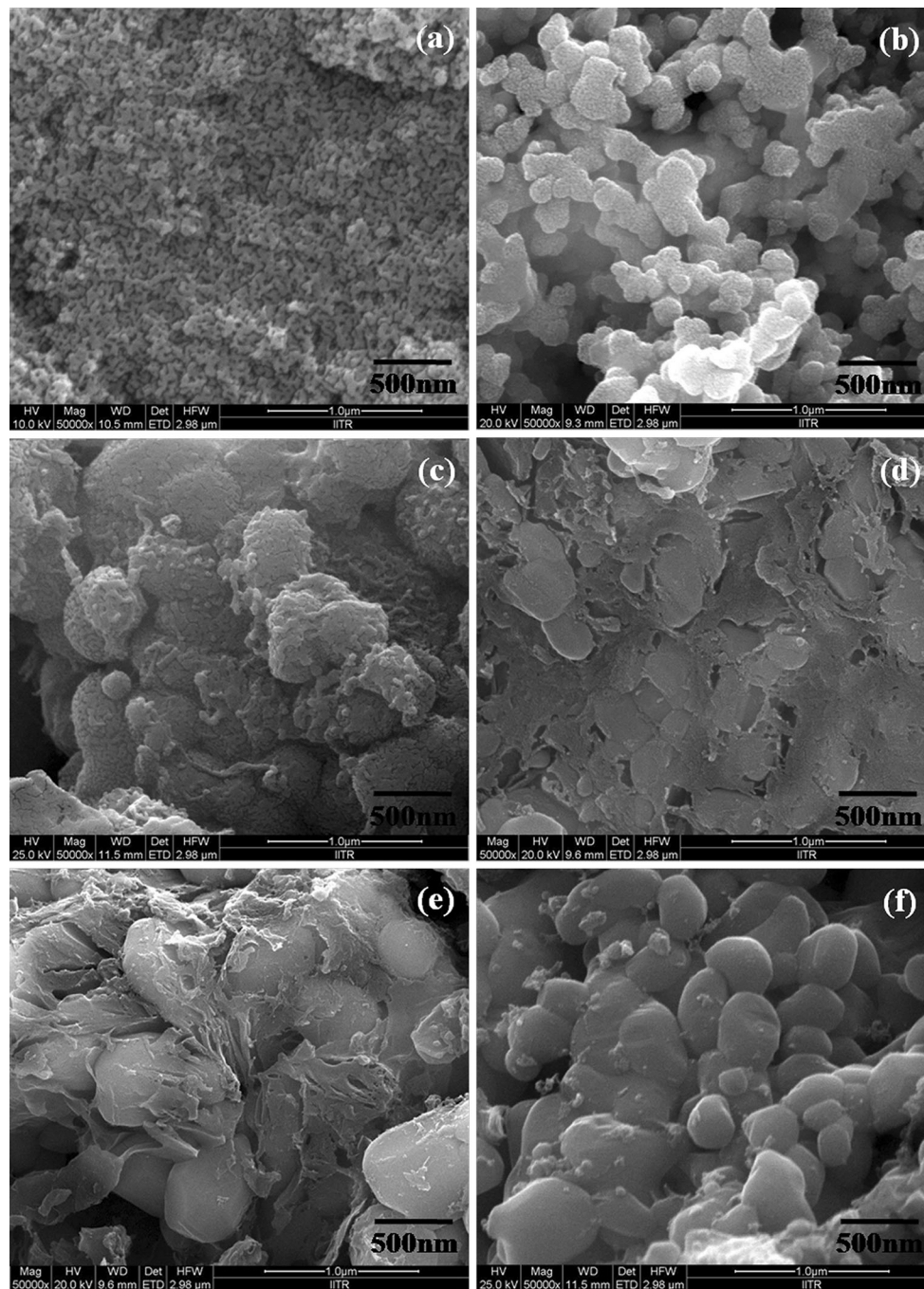


Fig. 3 SEM micrographs showing morphology of **a** PPy synthesized in ACN, **b** PPy synthesized in water, **c** LiFePO₄/C-PPy(ACN), **d** LiFePO₄/C-PPy(water), **e** LiFePO₄/C-PPy(ethanol) and **f** LiFePO₄/C

of the D-band and G-band indicates higher fraction of graphitic carbon and hence higher conductivity. The Fig. 5 shows the Gaussian fittings of the Raman spectra with deconvolution of D-band and G-band for LiFePO₄/C and LiFePO₄/C-PPy composites to measure the R values. The values of R for LiFePO₄/C, LiFePO₄/C-PPy(water), LiFePO₄/C-PPy (ethanol) and LiFePO₄/C-PPy (ACN) are 0.97, 0.77, 0.74 and 0.67 respectively. The decrease in R

values for all LiFePO₄/C-PPy composites shows improved graphitic carbon as compared to LiFePO₄/C. This is attributed to formation of H-bonds as a result of interaction between PPy and defect sites of carbon [19]. H-bonding occurs when nearly spherical shape ceramic particles were coated with polymer chains [20]. A minimum value (0.67) of R has been obtained for LiFePO₄/C-PPy(ACN). This is because polypyrrole coating of minimum porosity grown in

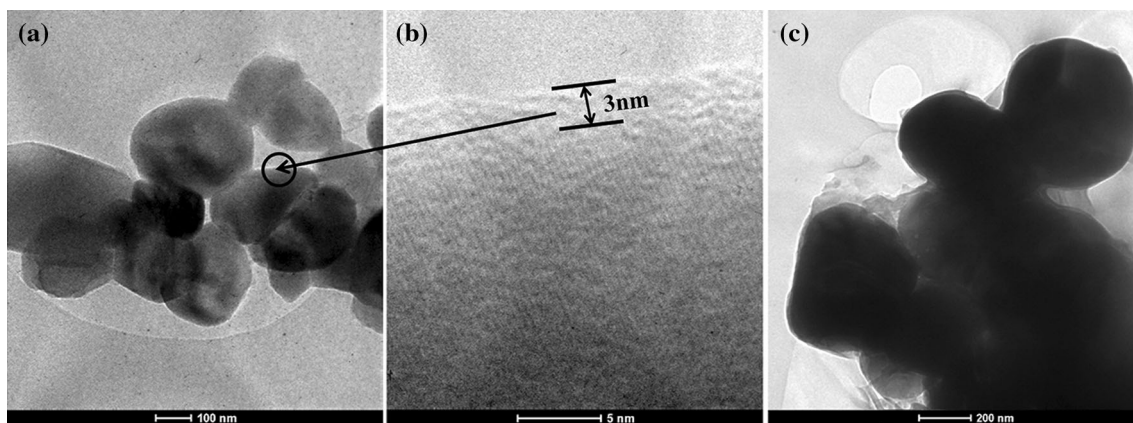


Fig. 4 TEM micrographs of **a** LiFePO_4/C powder, **b** magnified view of the micrograph (a), and **c** $\text{LiFePO}_4/\text{C-PPy(ACN)}$ powder

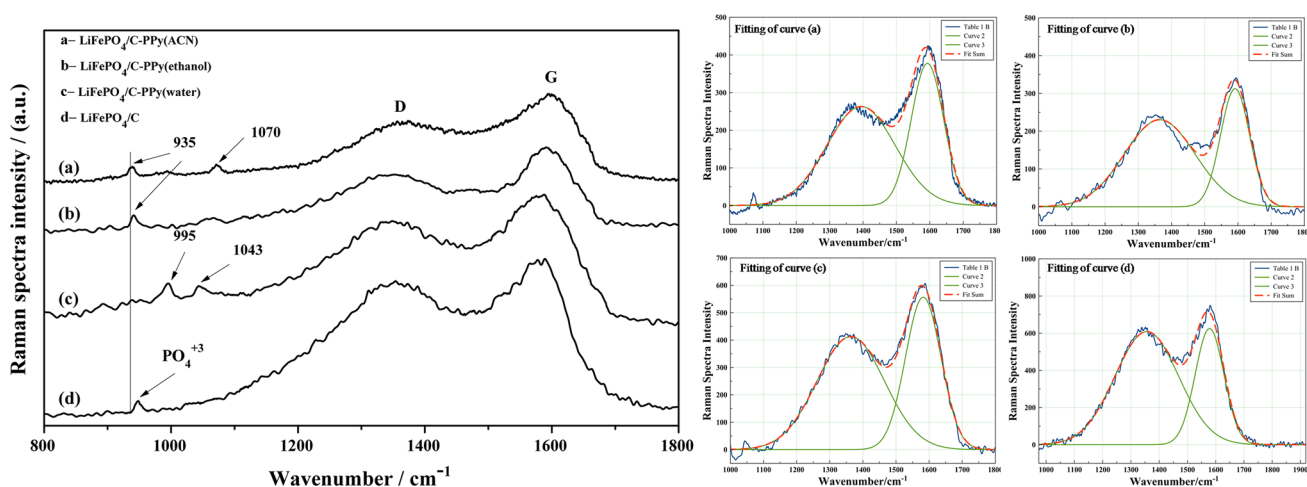


Fig. 5 Raman spectra of LiFePO_4/C and $\text{LiFePO}_4/\text{C-PPy}$ composites with their Gaussian fit and de-convoluted D-band and G-band

ACN solvent offers highest contact area with carbon coating. Hence large number of defects was interacted with PPy coating resulting decreased D-band intensity for $\text{LiFePO}_4/\text{C-PPy(ACN)}$ composite.

The growth of PPy was confirmed by the Raman spectra analysis (Fig. 5) of $\text{LiFePO}_4/\text{C-PPy}$ composites. Raman spectrum of $\text{LiFePO}_4/\text{C-PPy(water)}$ composite has weak bands at 995 and 1043 cm^{-1} . The band at 995 cm^{-1} is associated with the ring deformation vibration which has a consequence of polaron formation. The low intensity peak at 1043 cm^{-1} is assigned to symmetric C–H in-plane bending vibration in the benzoid ring [21]. The peaks at 935 and 937 cm^{-1} for the composites $\text{LiFePO}_4/\text{C-PPy(ACN)}$ and $\text{LiFePO}_4/\text{C-PPy(ethanol)}$ respectively arise due to C–H out of plane deformation in the quinoid ring and represent the bipolaron state of PPy [22]. The peak located at 1070 cm^{-1}

for $\text{LiFePO}_4/\text{C-PPy(ACN)}$ arise due to the C–H in-plane bending vibration occurred in the oxidized state of PPy. Although polaron and bipolaron states give rise to the conductivity of PPy, but bipolaron state favors the higher conductivity as compared to the polaron state [23]. Even though a single bipolaron peak at 935 cm^{-1} was observed for $\text{LiFePO}_4/\text{C-PPy(ethanol)}$, but the detection of two peaks at 935 and 1070 cm^{-1} reflects the higher oxidation of PPy in $\text{LiFePO}_4/\text{C-PPy(ACN)}$ which supports the higher conductivity.

3.6 EIS testing

EIS analyses were made to investigate the effect of solvents on the conductivity of the LiFePO_4/C and all $\text{LiFePO}_4/\text{C-PPy}$ electrode materials. Figure 6a shows the EIS profiles of LiFePO_4/C and $\text{LiFePO}_4/\text{C-PPy}$ composite

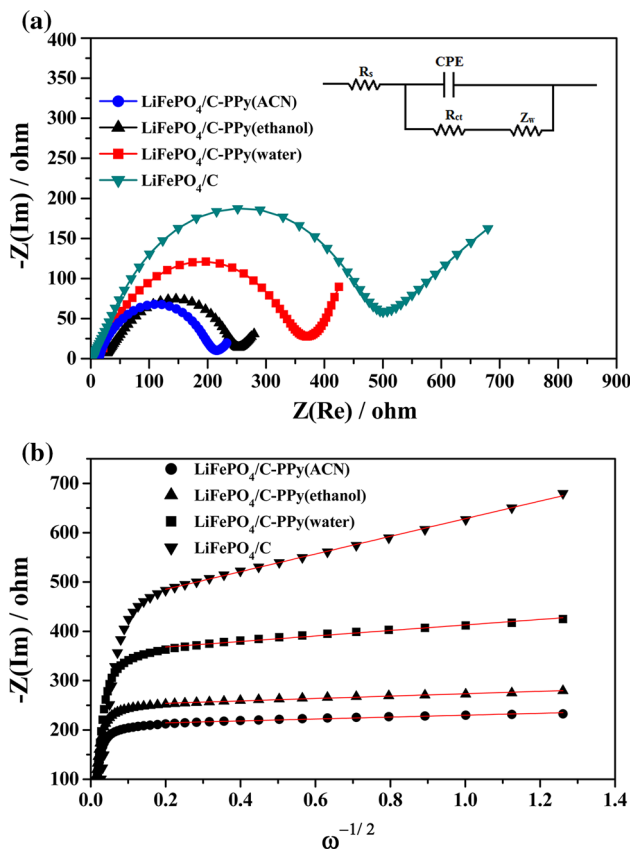


Fig. 6 a Electrochemical impedance spectra of LiFePO₄/C, LiFePO₄/C-PPy(water), LiFePO₄/C-PPy(ethanol) and LiFePO₄/C-PPy(ACN), b linear fitting of Warburg impedance

electrodes after five cycles of charging and discharging at 1 C rate. The measurements were performed at room temperature over the test frequencies between 0.1 Hz and 100 kHz. The EIS profiles can be explained with the help of equivalent circuit as shown in the inset of Fig. 6a. The equivalent circuit has a resistance (R_s) in series with a parallel combination of double-layer capacitance (C_{dl}), and charge transfer resistance (R_{ct}) in series with Warburg impedance (Z_w) [24]. Intercept of the semi-circle with Z_{real} in the high frequency region represents the ohmic resistance (R_s) which corresponds to interfacial resistance between the electrolyte and electrode. The intercept of semi-circle in the intermediate frequency range represents the charge transfer resistance (R_{ct}). A double layer capacitance was introduced to represent the constant phase element. The line in the low frequency region represents the Warburg impedance (Z_w) which corresponds to the Li-ion diffusion in the LiFePO₄ particles [25].

The low frequency response of EIS corresponds to the transport of Li-ion and electron into the electrode material [26]. So the diffusivity of Li-ion has been widely reported in the low frequency region of EIS using the expression [26, 27].

$$D_{Li^+} = \frac{R^2 T^2}{2A^2 n^4 F^4 c^2 \sigma_\omega^2} \tag{3}$$

Herein R is gas constant ($8.314 \text{ J mol}^{-1} \text{ K}^{-1}$), T is absolute temperature (300 K) of electrode during measurement, A is area of cathode–electrolyte interface, n is the number of electrons per molecule during oxidization (for LiFePO₄, $n = 1$), F is the Faraday constant ($96,487 \text{ C mol}^{-1}$), c is the molar concentration of lithium ion ($1.57 \times 10^{-2} \text{ mol cm}^{-3}$), σ_ω is the Warburg factor.

Warburg factor can be calculated from the following relation:

$$Z_{real} = R_s + R_{ct} + \sigma_\omega \omega^{-1/2} \tag{4}$$

The slope of the plot Z_{real} versus $\omega^{-1/2}$ in Fig. 6b in the low frequency region yields the σ_ω where ω is the angular frequency of the applied alternating current. The slopes of the linear fitting of the points in the low frequency region have been listed in the Table 2 for each sample. Using the relations (3) and (4), the calculated values of Li-ion diffusion coefficient are 7.37×10^{-15} , 7.56×10^{-14} , 4.00×10^{-13} and $6.23 \times 10^{-13} \text{ cm}^2 \text{ s}^{-1}$ for the samples LiFePO₄/C, LiFePO₄/C-PPy(water), LiFePO₄-PPy(ethanol) and LiFePO₄/C-PPy(ACN) respectively at room temperature. The calculated values of diffusivity show improvement as compared to 7.56×10^{-14} and $1.26 \times 10^{-14} \text{ cm}^2 \text{ s}^{-1}$ reported in the literature for LiFePO₄/C composite [28, 29]. The highest Li-ion diffusivity for LiFePO₄/C-PPy(ACN) composite can be explained by the Raman analysis. The interaction between PPy and defect sites of carbon coating reduces the interaction of Li-ion with the defect sites. The reduced interaction facilitates smooth movement of Li-ion on the graphitic carbon resulting higher diffusivity to the LiFePO₄/C-PPy(ACN) material [30].

The exchange current density is a factor which also reflects the electrochemical reversibility of the electrode and can be obtained from the following relation [31].

$$i_0 = \frac{RTA}{nFR_{ct}} \tag{5}$$

For all the synthesized materials, values of i_0 are calculated from the relation (5) and listed in the Table 2. The composite LiFePO₄/C-PPy(ACN) has the highest exchange current density $1.20 \times 10^{-4} \text{ mA cm}^{-2}$ of all the composite materials studied, reflecting best electrochemical reversibility. The improved exchange current density of 1.01×10^{-4} and $1.20 \times 10^{-4} \text{ mA cm}^{-2}$ was reported by ammonia assisted LiFePO₄/C and Na–Ti doping in LiFePO₄/C respectively [31, 32]. The minimum R_{ct} value was obtained for LiFePO₄/C-PPy(ACN) and consequently electronic conductivity of this composite material is highest among all the composites prepared.

Table 2 EIS parameter of electrodes of LiFePO₄/C, LiFePO₄/C-PPy(water), LiFePO₄/C-PPy(ethanol) and LiFePO₄/C-PPy(ACN)

Sample	R _s (Ω)	R _{ct} (Ω)	i ₀ (mA cm ⁻²)	D _{Li+} (cm ² s ⁻¹)	Slope
LiFePO ₄ /C	4.84	500.3	5.17 × 10 ⁻⁵	7.37 × 10 ⁻¹⁵	179.1
LiFePO ₄ /C-PPy(water)	13.4	368.8	7.01 × 10 ⁻⁵	7.56 × 10 ⁻¹⁴	55.9
LiFePO ₄ /C-PPy(ethanol)	19.7	252.0	1.02 × 10 ⁻⁴	4.00 × 10 ⁻¹³	24.31
LiFePO ₄ /C-PPy(ACN)	14.94	215.6	1.20 × 10 ⁻⁴	6.23 × 10 ⁻¹³	19.4

The higher electronic conductivity of the sample LiFePO₄/C-PPy(ACN) over samples LiFePO₄/C-PPy(water) and LiFePO₄/C-PPy(ethanol) was attributed to the following effects. (1) The bipolaron formation in PPy coating in ACN solvent as compared to polaron formation in water. (2) Generation of -OH and C = O groups during polymerization of pyrrole in water and ethanol solvents restrict the delocalization of polaron and bipolaron [15]. (3) The generated -OH and C = O groups during the synthesis attack on the active sites which restricts the PPy chain growth mechanism and resulting in the higher porosity [15]. On the other hand, higher porosity generated during the synthesis of PPy produce the discontinuity in the surface coating and hence larger path length for the conducting species. As a result Fig. 6a shows LiFePO₄/C-PPy(ACN) composite giving minimum R_{ct} = 215.6 Ω as compared to 500.3, 368.8 and 252.0 Ω for samples LiFePO₄/C, LiFePO₄/C-PPy(water) and LiFePO₄/C-PPy(ethanol) respectively.

3.7 Electrochemical analysis

The discharge profiles of the cathode materials LiFePO₄/C-PPy(ACN), LiFePO₄/C-PPy(ethanol), and LiFePO₄/C-PPy(water) measured at 0.2, 0.5, 1, 2, 5, 10 and 20 C-rates are presented in a manner comparative with that of LiFePO₄/C, in Fig. 7a–c. It is seen that the rate capability has enhanced for all the PPy coated composites as compared to LiFePO₄/C. For LiFePO₄/C-PPy(ACN), LiFePO₄/C-PPy(ethanol), LiFePO₄/C-PPy(water) and LiFePO₄/C materials the discharge capacities are 139, 137, 138 and 142 mAh g⁻¹ respectively obtained at low C-rate (0.2 C), and 82, 60, 54 and 42 mAh g⁻¹ respectively at high C-rate (20 C). The measurements at 5, 10 and 20 C-rates for the composite LiFePO₄/C-PPy(ACN) show discharge capacities of 98, 91 and 82 mAh g⁻¹ respectively. However the discharge capacities of LiFePO₄/C-PPy(ethanol) at 5, 10 and 20 C-rates are 83, 71 and 60 mAh g⁻¹ respectively. The enhanced rate capability of LiFePO₄/C-PPy composite material synthesized electrochemically was reported by Huang et al. [33]. All the LiFePO₄/C-PPy composites show a minor decrease in discharge capacity at low current rates. At low current rates the discharge capacities of LiFePO₄/

C-PPy and LiFePO₄/C are comparable as PPy coating do not have significant effect on the conduction because of slow movement of charge species. However the difference in capacities has substantially increased when current is increased up to 20 C. From Fig. 7a–c one can infer that LiFePO₄/C-PPy(ACN) has higher rate capability than other counter parts synthesized in water and ethanol solvents. In order to investigate the higher capacity of LiFePO₄/C-PPy(ACN) conductivity measurements of all the samples were made and the results are consistent with the electrochemical measurements. The low electronic conductivity of the LiFePO₄/C-PPy(water) and LiFePO₄/C-PPy(ethanol), and improved Li-ion diffusion in the LiFePO₄/C-PPy(ACN) composite was supported by morphological and structural analysis of the PPy coating.

It has been reported in many studies [30, 34] that higher number of defects on carbon coating offers more sites to occupy Li-ions, but there may be no de-intercalation from these sites due to which less number of Li-ions participate in the charging/discharging process, resulting increased irreversible capacity. The Raman analysis confirmed the minimum number of defects on the carbon for LiFePO₄/C-PPy(ACN) which may be occupied by the Li-ions and contribute to the lowest irreversible capacity followed by LiFePO₄/C-PPy(ethanol) and LiFePO₄/C-PPy(water). The Fig. 7d compares the discharge capacities for all the LiFePO₄/C-PPy(ACN), LiFePO₄/C-PPy(ethanol) and LiFePO₄/C-PPy(water) composites at typically 2 C-rate for 50 cycles. All the LiFePO₄/C-PPy samples shows superior cyclability in comparison with LiFePO₄/C. The capacity fade of 2, 5, 9 11 % as compared to initial capacity were observed for LiFePO₄/C-PPy(ACN), LiFePO₄/C-PPy(ethanol), LiFePO₄/C-PPy(water) and LiFePO₄/C samples respectively over 50 cycles. This shows that PPy addition to LiFePO₄/C improves the cyclability and rate capability for all the solvents.

Figure 8a shows the discharge capacities of the materials measured at different C-rates and for every C-rate, measurements were made for five cycles. In order to investigate the rate capability of composites LiFePO₄/C-PPy(ACN), LiFePO₄/C-PPy(ethanol) and LiFePO₄/C-PPy(water), a factor 'differential capacity (DC)' as expressed below, has been devised.

$$DC = \frac{\text{Discharge capacity of LiFePO}_4\text{/C(PPy)} - \text{Discharge capacity of LiFePO}_4\text{/C}}{\text{Discharge capacity of LiFePO}_4\text{/C}} \quad (6)$$

The Fig. 8b represents the plot of differential capacity (DC) versus C-rate. From the graph it can be inferred that the DC values are very close to zero, at lower discharging rates of 0.2 and 0.5 C respectively. At moderate discharge rates of 1, 2 and 5 C the DC of each samples start spreading and shows maximum spread at highest 20 C rate. The sample LiFePO₄/C-PPy(water) have a slight dip in DC at 10 C rate showing a decrease in the rate capability as compared to 5 C. The highest DC value of 1.08 have been obtained for LiFePO₄/C-PPy(ACN) composite material at 20 C rate implying that it is a high rate capability material followed by LiFePO₄/C-PPy(Ethanol) and LiFePO₄/C-PPy(Ethanol).

Figure 9a shows the discharge capacity of pure PPy synthesized in water, ethanol and ACN solvents, relative to cell voltage. The profile of graph shows that the PPy

samples are electrochemically active in the range of 4.2–2.0 V, delivering the specific discharge capacities of 61, 64 and 68 mAh g⁻¹ for water, ethanol and ACN solvents respectively at 1 C rate. The discharge capacity of PPy is highest for ACN solvent followed by those prepared in ethanol and water. This was due to the fact that electronic conductivity and Li-ion diffusivity were affected by the solvent and morphology of PPy. The continuous nature of PPy coating derived in ACN solvent is the reason for higher capacity of the composite. In both coating and bulk, PPy synthesized in ACN has denser structure as compared to that prepared in water and ethanol solvents. The discontinuity (Fig. 2b) restricts the flow of conducting species due to which the overall conductivity of material decrease [15]. So, a continuous coating is required to achieve good conductivity of the material. The discharge capacity of the

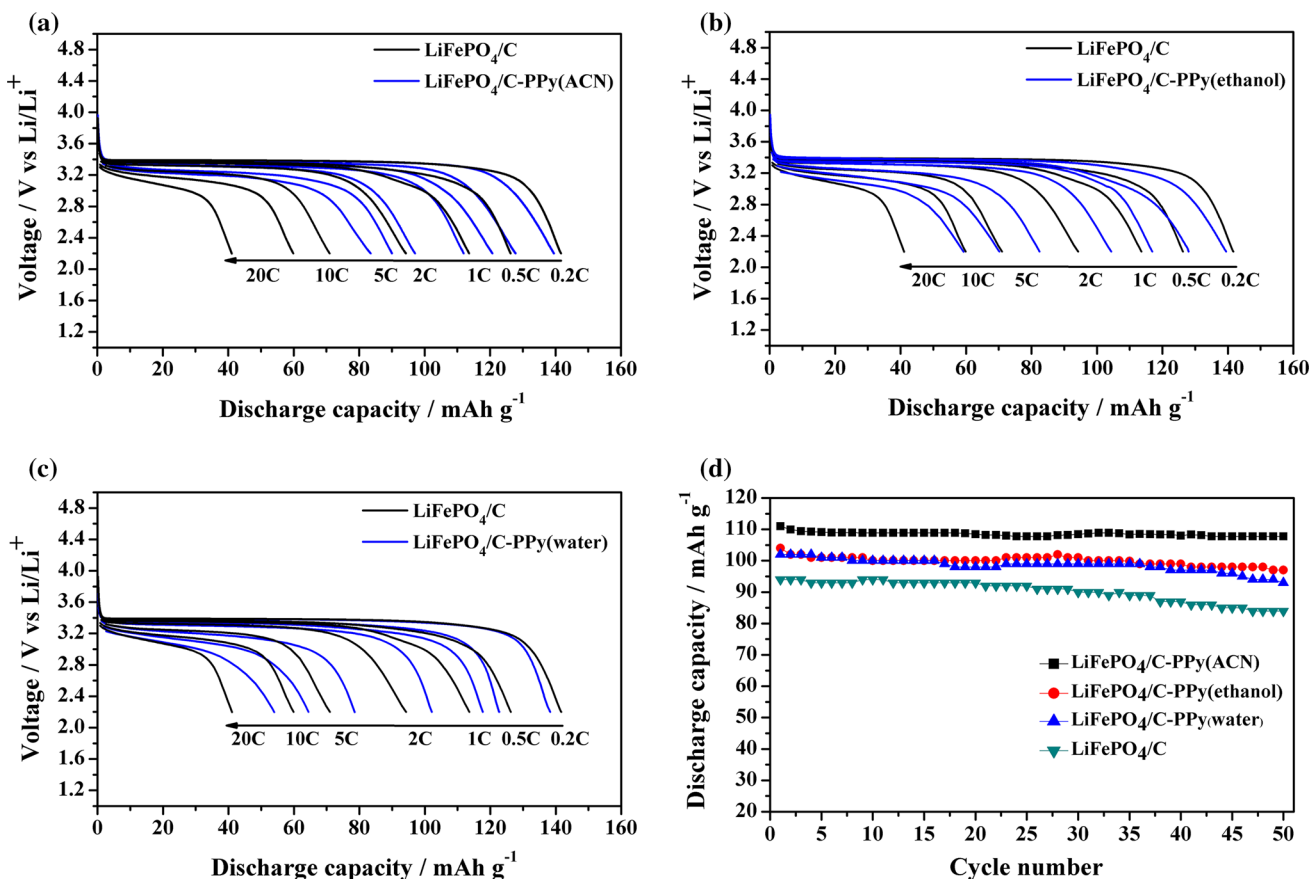


Fig. 7 Comparative plots of the capacities of composites **a** LiFePO₄/C-PPy(ACN), **b** LiFePO₄/C-PPy(ethanol), **c** LiFePO₄/C-PPy(water) with LiFePO₄/C. **d** Discharge capacities of LiFePO₄/C and LiFePO₄/C-PPy composites at 2 C rate for 50 cycles

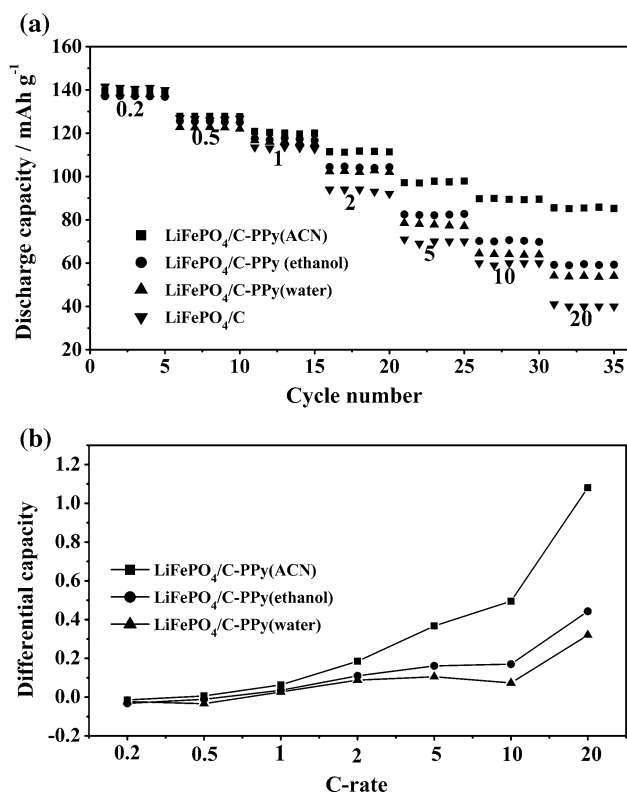


Fig. 8 **a** Discharge capacity of LiFePO₄/C-PPy(ACN), LiFePO₄/C-PPy(ethanol), LiFePO₄/C-PPy(water) and LiFePO₄/C for five cycles at different rate of 0.2, 0.5, 1, 2, 5, 10 and 20 C, **b** differential capacities variation with C-rate

polymers synthesized in different solvents with respect to cycle number is given in the Fig. 7b for 20 cycles. The discharge capacities of PPy synthesized in ACN is almost constant. However, water and ethanol solvents deliver 92 and 96 % of the initial capacity respectively, after 20 cycles, showing the maximum stability of PPy synthesized in ACN.

4 Conclusions

The material LiFePO₄/C has been prepared by chemical precipitation method followed by calcinations in the presence of Ar-10 %H₂ atmosphere. The polypyrrole coating on the surface of LiFePO₄/C has been produced by chemical oxidation method using FeCl₃ as oxidizing agent in different solvents viz. water, ethanol, and ACN. The composite LiFePO₄/C-PPy(ACN) produces appreciable rate capability of 82 mAh g⁻¹ at 20 C. The superior electrochemical performance of the LiFePO₄/C-PPy(ACN) is attributed to the better electronic conductivity and enhanced Li-ion diffusion. The composite LiFePO₄/C-PPy(ACN) shows better electronic conductivity due to the bipolaron formation within the PPy chains. The formation

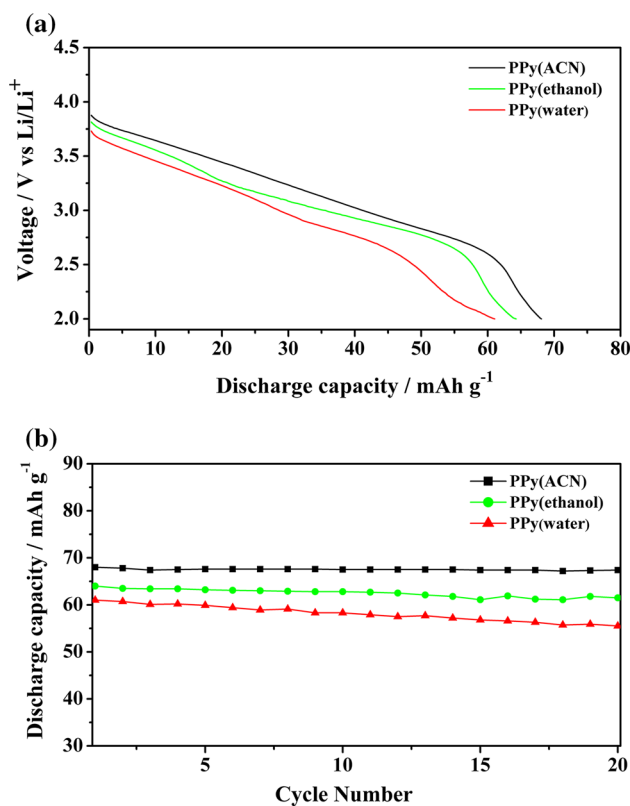


Fig. 9 **a** Voltage versus discharge capacity and **b** discharge capacity versus number of cycles of PPy synthesized in water, ethanol and ACN solvents at 1.0 C rate

of -OH and C = O groups during polymerization depreciate conductivity for samples LiFePO₄/C-PPy(water) and LiFePO₄/C-PPy(ethanol) on the other hand the formation of bipolaron supports the higher electronic conductivity for LiFePO₄/C-PPy(ACN). The improved Li-ion diffusion for LiFePO₄/C-PPy(ACN) was attributed to the reduced interaction offered by the decreased number of defect sites on carbon coating.

References

1. C.W. Ong, Y.K. Lin, J.S. Chen, *J. Electrochem. Soc.* **154**, A527 (2007)
2. S.Y. Chung, J.T. Bloking, Y.M. Chiang, *Nat. Mater.* **1**, 123 (2002)
3. B. Jin, H.B. Gu, W. Zhang, K.H. Park, G. Sun, *J. Solid State Electrochem.* **12**, 1549 (2008)
4. Z. Yang, J. Xia, L. Zhi, W. Zhang, B. Pei, *Ionics* **20**, 169 (2014)
5. Y. Chen, J. Mao, *J. Mater. Sci. Mater. Electron.* **25**, 5153 (2014)
6. Z. Chena, J.R. Dahna, *J. Electrochem. Soc.* **149**, A1184 (2002)
7. Z. Liu, S.W. Tay, L. Hong, J.Y. Lee, *J. Solid State Electrochem.* **15**, 205 (2011)
8. A.K. Wanekaya, Y. Lei, E. Bekyarova, W. Chen, R. Haddon, A. Mulchandani, N.V. Myung, *Electroanalysis* **18**, 1047 (2006)
9. S. Machida, S. Miyata, *Synth. Met.* **31**, 311 (1989)

10. A. Kaynak, *Fibers. Polym.* **10**, 590 (2009)
11. K.A. Noh, D.W. Kim, C.S. Jin, K.H. Shin, J.H. Kim, J.M. Ko, *J. Power Sources* **124**, 593 (2003)
12. L. Yuan, J. Wang, S.Y. Chew, J. Chen, Z.P. Guo, L. Zhao, K. Konstantinov, H.K. Liu, *J. Power Sources* **174**, 1183 (2007)
13. A. Yamada, H. Koizumi, S.I. Nishimura, N. Sonoyama, R. Kanno, M. Yonemura, T. Nakamura, Y. Kobayashi, *Nat. Mater.* **5**, 357 (2006)
14. I. Rodriguez, B.R. Scharifker, J. Mostany, *J. Electroanal. Chem.* **491**, 117 (2000)
15. J.M. Ko, H.W. Rhee, S.M. Park, C.Y. Kim, *J. Electrochem. Soc.* **137**, 905 (1990)
16. M.S. Dresselhaus, A. Jorio, R. Saito, *Annu. Rev. Condens. Matter Phys.* **1**, 89 (2010)
17. F. Tuinstra, J.L. Koenig, *J. Chem. Phys.* **53**, 1126 (1970)
18. J. Li, Q. Qu, L. Zhang, L. Zhang, H. Zheng, *J. Alloy Compd.* **579**, 377 (2013)
19. M.L. Singla, R. Sehrawat, N. Rana, K. Singh, *J. Nanopart. Res.* **13**, 2109 (2011)
20. T. Tanaka, M. Kozako, *I.E.E.E. Trans, Dielectr. Electr. Insul.* **12**, 669 (2005)
21. M. Li, Z. Wei, L. Jiang, *J. Mater. Chem.* **18**, 2276 (2008)
22. J. Duchet, R. Legras, S.D. Champagne, *Synth. Met.* **98**, 113 (1998)
23. Y. Hou, L. Zhang, L.Y. Chen, P. Liu, A. Hirata, M.W. Chen, *Phys. Chem. Chem. Phys.* **16**, 3523 (2014)
24. F. Gao, Z. Tang, *Electrochim. Acta* **53**, 5071 (2008)
25. A.Y. Shenouda, H.K. Liu, *J. Power Sources* **185**, 1386 (2008)
26. J. Song, M.Z. Bazant, *J. Electrochem. Soc.* **160**, A15 (2013)
27. Y. Xia, W.K. Zhang, H. Huang, Y.P. Gan, C.G. Li, X.Y. Tao, *Mater. Sci. Eng. B* **176**, 633 (2011)
28. C. Chen, G.B. Liu, Y. Wang, J.L. Li, H. Liu, *Electrochim. Acta* **113**, 464 (2013)
29. H. Shu, X. Wang, Q. Wu, L. Liu, Q. Liang, S. Yang, B. Ju, X. Yang, X. Zhang, Y. Wang, Q. Wei, B. Hu, Y. Liao, H. Jiang, *Electrochim. Acta* **76**, 120 (2012)
30. M. Jana, A. Sil, S. Ray, *J. Phys. Chem. Solids* **75**, 60 (2014)
31. J. Lee, P. Kumar, J. Lee, B.M. Moudgil, R.K. Singh, *J. Alloy Compd.* **550**, 536 (2013)
32. H. Shu, X. Wang, W. Wen, Q. Liang, X. Yang, Q. Wei, B. Hu, L. Liu, X. Liu, Y. Song, M. Zho, Y. Bai, L. Jiang, M. Chen, S. Yang, J. Tan, Y. Liao, H. Jiang, *Electrochim. Acta* **89**, 479 (2013)
33. Y.H. Huang, K.S. Park, J.B. Goodenough, *J. Electrochem. Soc.* **153**, A2282 (2006)
34. M. Winter, P. Novak, A. Monnier, *J. Electrochem. Soc.* **145**, 428 (1998)